

Rocksalt phase and superconductivity in pressurized SnSe

Xuliang Chen,¹ Xuefei Wang,¹ Yonghui Zhou,¹ Chao An,¹ Ying Zhou,¹
 Cong Xian,¹ Binyang Hou,² Changyong Park,² Kunling Peng,³ Xiaoyuan
 Zhou,³ Yimin Xiong*,^{1,4} Zhaorong Yang*,^{1,4,5} and Yuheng Zhang^{1,4}

¹*High Magnetic Field Laboratory, Chinese Academy of Sciences and
 University of Science and Technology of China, Hefei 230031, China*

²*High Pressure Collaborative Access Team, Geophysical Laboratory,
 Carnegie Institution of Washington, Argonne, Illinois 60439, USA*

³*College of Physics, Chongqing University, Chongqing 401331, China*

⁴*Collaborative Innovation Center of Advanced Microstructures, Nanjing, 210093, China*

⁵*Key Laboratory of Materials Physics, Institute of Solid State Physics,
 Chinese Academy of Sciences, Hefei 230031, China*

(Dated: November 28, 2018)

* Corresponding authors (emails): yxiong@hmfll.ac.cn or zryang@issp.ac.cn

Abstract

Recently, SnTe material class with rocksalt structure has been attracting renewed interest due to the newly reported topological states of matter, referred to topological crystalline insulators (TCIs), in which the topological nature of electronic structures stems from the crystal symmetries. SnSe, a sister compound of SnTe, crystallizes in a heavily distorted orthorhombic structure at ambient conditions and thus is not a TCI. However, SnSe with a rocksalt structure has been predicted to be a native TCI theoretically. To date, the rocksalt SnSe experimentally achieved is only limited to epitaxial films where Dirac surface states are observed [Wang *et al.*, Adv. Mater. **27**, 4150 (2015)]. Here we report a formation of the rocksalt SnSe at high pressures, observed by synchrotron X-ray diffraction up to 50.1 GPa in a diamond anvil cell. We also report our discovery of a pressure-induced superconductivity accompanied by the appearance of the rocksalt phase through electrical transport measurements up to 55.0 GPa. Based on these results, a new candidate system to realize topological superconductivity is highly expected. Our findings offer an important clue to the synthesis of rocksalt SnSe that is stable at ambient conditions by a combination of high temperature and high pressure techniques.

INTRODUCTION

Topological crystalline insulators (TCIs), a new category of topological materials, were predicted[1, 2] and confirmed experimentally in rocksalt (NaCl-type) SnTe and $\text{Pb}_{1-x}\text{Sn}_x\text{Te}(\text{Se})$ by angle-resolved photoemission spectroscopy (ARPES)[3–6]. In contrast to topological insulators where the gapless metallic surface state is protected by time-reversal symmetry, TCIs have multiple Dirac surface states and their topological characteristics are protected by crystalline symmetries[7]. These surface states can generate a continuously tunable band gap by applying electric field or alloying to break the crystalline symmetry[5, 8, 9], shedding light on future applications of electronic and spintronic devices. Based on TCIs, superconductivity was achieved successfully in In-doped SnTe[10–14] and $\text{Pb}_{0.5}\text{Sn}_{0.5}\text{Te}$ [15]. In the $\text{Sn}_{1-x}\text{In}_x\text{Te}$ superconductor, surface Andreev bound states were observed by ARPES, which was related to odd-parity pairing and topological superconductivity[10]. Most recently, unexpected superconductivity was reported in TCI $\text{Pb}_{0.6}\text{Sn}_{0.4}\text{Te}$ by forming a mesoscopic point-contact using a normal non-superconducting elemental metal on its surface[16]. The above experimental evidences suggest that TCIs may be a promising platform to realize topological superconductivity.

SnSe, as one of the parent compounds, is known as a material with excellent thermoelectric properties above room temperature[17, 18]. Under ambient conditions, it has the orthorhombic GeS-type structure [18, 19] and thus is not a TCI due to the broken mirror symmetry[9]. A recent theoretical study however, has shown that SnSe with the rocksalt structure could be a native TCI[20]. Due to the small energy difference between the orthorhombic and rocksalt structures[20], it is readily expected that SnSe with the rocksalt structure could be obtained experimentally. Indeed, Wang *et al.* have reported the successful synthesis of rocksalt SnSe in epitaxial films, where the nontrivial topology is confirmed in terms of the observation of Dirac surface states by ARPES[21]. As one of the fundamental state parameters, high pressure is a clean and effective way to tune lattice as well as electronic states[22–29]. While it has undergone extensive investigations during the past several decades[30–36], SnSe with the rocksalt structure under pressure has not been reported yet. One may note that the highest pressure investigated in these studies is generally smaller than 30 GPa, which probably limits the formation of rocksalt SnSe under compression.

In the present work, by extending the pressure up to 50.1 GPa in a diamond anvil cell

and using synchrotron X-ray diffraction (XRD), we observe two structural transitions for SnSe: the starting orthorhombic $Pnma$ structure transforms into another orthorhombic $Bbmm$ one (or equivalently $Cmcm$) between 15.5 and 19.3 GPa and further to a high pressure rocksalt $Fd\bar{3}m$ structure. The latter transition involves a large broad mixture of the $Bbmm$ and $Fd\bar{3}m$ structures from 27.3 to 43.4 GPa and above 50.1 GPa the rocksalt phase establishes completely. We also observe a pressure-induced superconductivity along with the appearance of the rocksalt phase, through electrical transport measurements up to 55.0 GPa. The observation of both rocksalt structure and superconductivity at high pressures indicates that dense SnSe could be a topological superconductor candidate and is worthy of further theoretical and experimental investigations.

RESULTS

Structural phase transitions under pressure

To search for the possible rocksalt SnSe at high pressure, *in situ* synchrotron X-ray diffraction (XRD) experiments were performed with SnSe sample up to 50.1 GPa at room temperature ($\lambda = 0.4246 \text{ \AA}$). The experimental results are presented in Fig. 1. Standard Rietveld refinements were performed using GSAS program[37]. Starting at 1.3 GPa, the pattern can be indexed solely by the GeS-type orthorhombic structure with space group $Pnma$ (No. 62), which is the same as that of SnSe at ambient conditions[38]. With increasing pressure, we have identified three different phases during compression to 50.1 GPa: the low pressure Phase I remains only to 15.5 GPa (black); a pure Phase II shows up in the pressure region of 19.3-23.0 GPa (red); a broad mixture region of Phases II and III exists from 27.3 to 43.4 GPa (yellow); and above 50.1 GPa, a pure Phase III forms (blue). It should be noted that when decompressing back to 0.3 GPa (denoted by D), the XRD pattern came back to the starting structure, manifesting that the pressure-driven structural transition is reversible.

We have determined that the lattice structure of Phase II is described by space group $Bbmm$ (No. 63) or a non-standard setting of space group $Cmcm$ (No. 63) that maintains the crystal axes in the same orientation as for the low pressure $Pnma$ structure. Such structural transition of $Pnma \rightarrow Bbmm$ (or $Cmcm$) under pressure was also reported by previous work in bulk SnSe[31]. Whereas, the critical pressure in the present study (at least

> 15.5 GPa) is higher than the value (10.5 GPa) obtained previously[31]. This discrepancy seems to be due to the sample dependency[32, 33]. At 50.1 GPa, the XRD profile for Phase III can be indexed by a rocksalt NaCl-type structure with space group $Fm\bar{3}m$ (No. 225). In the pressure range of 27.3-43.4 GPa, the XRD pattern is a superposition of the $Bbmm$ and $Fm\bar{3}m$ structures. Selected XRD profile refinements are presented in Fig. S1 and the corresponding fitting parameters are summarized in TABLE S1.

Figure 2a shows the variations in lattice parameters as a function of pressure. In Phase I, with increasing pressure all of the lattice parameters decrease gradually. However, the a lattice parameter is apparently more compressible than the two others, showing an anisotropic feature. This anisotropy can be related to the fact that the unit cell of SnSe is composed of bilayers perpendicular to the direction of the longest axis (a in our case, see the left frame of Fig. 2b). And the van der Waals force dominates between adjacent layers while strong chemical bond links the atoms within the layer. On the other hand, the lattice parameters b and c continuously approach a same value from about 6 GPa. At about 11 GPa the axial ratio changes from $b/c < 1$ to $b/c > 1$. In Phase II, while the anisotropic compressibility remains, the difference between the parameters b and c keeps almost unchanged with pressure. Consequently, since the c axis is much stiffer than b axis (Fig. 2a), it thus is inferred that the transition from Phases I to II is related to a displacive movement of Sn/Se atoms along the $[010]$ direction (or b axis), which is in accordance with previous reports[31, 34]. Note that, over the transition, all the lattice parameters evolve almost smoothly with pressure, indicating the transition to be a second order. It is also interesting to see that the lattice of SnSe approaches a tetragonal metric around 11 GPa, but remains orthorhombic at all pressures for Phase I and Phase II. Such displacive structural transition and the modified tetragonal metric at high pressure are quite similar to those of SnSe at elevated temperature[38, 39].

Phase III starts to appear at 27.3 GPa and the lattice parameter “ a ” decreases slightly with pressure up to 50.1 GPa, the highest pressure achieved in the present XRD experiments. The discontinuous change of lattice parameters from phases II to III implies that the transition is a first order. A broad pressure region of coexistence between Phase II and III is observed, and thus it is hard to determine the exact critical pressure. Here the critical pressure from Phase II to III is defined as the one above which Phase III appears indicated by the dashed line in Fig. 2a. Based on the variation of lattice parameters with pressure from Phase II to III, one can find that the high pressure structural transition roughly involves

two factors: first, a gradual decreasing of the interlayer spacing; second, a lateral shifting of adjacent layers. And finally a bonding of Sn to Se from neighboring layers occurs, which makes the transition from a predominantly two-dimensional (2D) material (Phase II) to a three-dimensional (3D) network (Phase III), as illustrated in Fig. 2b.

The isothermal equations of state for Phase I, II and III are plotted in Fig. 2c. The isothermal equations of state were fitted by the third-order Birch-Murnaghan formula[40] as indicated by the solid lines. The calculated parameters are: the bulk moduli $B_0 = 39.8$ GPa, and its first derivative $B'_0 = 4.31$ for Phase I; $B_0 = 55.4$ GPa, and $B'_0 = 4.55$ for Phase II; and $B_0 = 94.9$ GPa, and $B'_0 = 4.83$ for Phase III. The estimated volume at zero pressure are $V_0 = 214.4 \text{ \AA}^3$ for Phase I, $V_0 = 198.0 \text{ \AA}^3$ for Phase II, and $V_0 = 120.0 \text{ \AA}^3$ for Phase III. The obtained B_0 of Phase I is in reasonable agreement with the reported experimental and theoretical values [31, 32, 34–36]. Note that the bulk moduli of Phase III is substantially larger than that of Phase II, which can be related to the observation of a pressure-induced 2D to 3D structural transition. In addition, the unit cell volume shrinks at a ratio as high as 33.5% for the high pressure transition but only 2% for the low pressure one. Such a large volume collapse phenomenon was also observed in previous high pressure XRD studies[41, 42].

Pressure-induced superconductivity

It is well known that, at ambient conditions, SnSe exists in a thermodynamically stable GeS-type orthorhombic structure. Here, high pressure SnSe with a rocksalt structure is rather interesting: first, rocksalt SnSe has been predicted theoretically to be a native TCI[20]; second, it stabilizes at ambient conditions via epitaxial film growth method, in which the Dirac surface states of the topological phase were successfully observed by ARPES experiments[21]. Since its topological nature of electronic states is protected only by lattice symmetry[20, 21], the rocksalt SnSe accessed by high pressure thus may be a candidate of a bulk TCI. To investigate its high pressure manifestations in electronic properties, we carried out electrical transport measurements on single crystal SnSe up to 55.0 GPa.

Figure 3 shows the temperature dependence of the *DC* electrical resistance of SnSe in the temperature range of 1.8 - 300 K. From Fig. 3a, at 0.4 GPa a semiconducting behavior ($dR/dT < 0$) is observed in the whole temperature range as that of semiconducting SnSe at ambient pressure[43]. With increasing pressure, the whole resistance decreases rapidly

implying a remarkable reduction in the energy gap of the material with pressure (see the Arrhenius fits to the resistance data in Fig. S2). From 5.4 to 9.0 GPa while the semiconducting behavior remains at high temperatures (above ~ 250 K), a metallic-like feature ($dR/dT > 0$) shows up at low temperatures. At 12.0 GPa, a typical metallic character is observed. At the same time, the resistance at 2 K drops about six orders of magnitude with respect to that at 0.4 GPa. These observations signal a crossover from semiconductor to metal under pressure. Recall that in above XRD experiments, from about 6 GPa the parameters b and c approach gradually to the same value (see Fig. 2a). In addition, a crossover from $b/c < 1$ to $b/c > 1$ was observed at about 11 GPa. As a result, there is a close correlation between the electrical and structural properties. Since the c axis is much stiffer than b axis, it thus can be inferred that the metallization of SnSe under pressure is related to the atomic displacement along the $[010]$ direction (or b axis). Here the critical pressure (12.0 GPa) of metallization for SnSe is in excellent accordance with the one (12.6 GPa) obtained from previous resistance experiments although the latter was performed in the temperature range of 80-270 K[36]. When the pressure goes up to 17.3 GPa, however, the resistance reveals an abnormal overall rise in addition to the metallic feature as indicated by the dashed line in Fig. 3b. This can be ascribed to the structural transition from Phase I to II, which is triggered by the displacive movement of Sn/Se atoms and the increase of the atomic coordination via bonding of the non-bonding in-plane Sn to Se atoms, along the $[010]$ direction (Fig. 2b).

Upon further compression, the resistance becomes more and more metallic. The most striking finding is that at 27.2 GPa a drop of resistance is initially observed below about 2.5 K as presented in Fig. 3c and in Fig. 3d, an enlarged view of the low temperature region of resistance. This sharp drop should be a signal of a superconducting transition as zero resistance is observed at 2 K at 34.3 GPa. The critical temperature, T_C , is defined as the onset of the superconducting phase transition. Further increasing pressure, it first increases slightly, reaches a maximum of about 3 K at 39.0 GPa and then decreases gradually to 2.5 K at 55.0 GPa, the highest pressure achieved in the present measurement. It should be noted here that the pressure-induced superconductivity is only observed being accompanied by the appearance of the high pressure rocksalt phase above about 27 GPa. Moreover, the magnitude of the resistance at low temperatures in the normal state keeps substantially unchanged, i.e. showing pressure- and temperature-independent behaviors (above 39.0 GPa; below ~ 70 K) within the experimental uncertainties.

To further confirm that the drop in resistance belongs to a superconducting transition, we measured the low temperature resistance at 39.0 GPa under applied magnetic fields parallel to the [100] direction, as displayed in Fig. 4a. With increasing field, T_C decreases gradually and the resistance drop was almost smeared out at 0.5 T, which confirms that the drop of resistance is the superconducting transition. In addition, the resistance versus temperature curves are almost parallel to each other, suggesting that the flux creep effects can be ignored in the vortex dynamics of superconductivity. We have plotted the upper critical field H_{C2} as a function of temperature in Fig. 4b. Here $H_{C2}(T)$ is defined from the resistance criterion of $R_{cri} = 90\%R_n$ (R_n is the normal state resistance). One can see that H_{C2} follows a linear dependence in temperature (red dashed line). By extrapolating it to zero temperature, $H_{C2}(0)$ is estimated to be 1.12 T. The linear feature of H_{C2} and the value of $H_{C2}(0)$ are quite similar to those observed in In-doped SnTe[12, 13] and $\text{Sn}_{0.8}\text{Ag}_{0.2}\text{Te}$ [14], potential candidates where topological superconductivity may emerge[10, 11]. Here, the Pauli paramagnetic effect does not apply since the Pauli limiting field is about 5.4 T ($1.84 \times T_C$), suggestive of an absence of Pauli pair breaking.

Phase diagram of SnSe under pressure

All of the results are outlined in a phase diagram as exhibited in Fig. 5. It is easy to find that the structural and electronic properties correlate with each other intimately in the whole pressure range studied. Roughly, the phase diagram can be divided into four different regions based on the lattice symmetry upon compression. For the low pressure $Pnma$ structure, the pristine semiconducting behavior gradually develops into a metallic state, with the resistance at 2 K (left axis of Fig. 5) and at room temperature (inset of Fig. 5) decreasing 4-6 orders in magnitude. When entering into the $Bbmm$ structure, the resistance exhibits a sudden increase as can be seen in Fig. 5 (left axis and inset) and more clearly in Fig. 3b. Then with increasing pressure it decreases continuously and becomes more and more metallic. Accompanied by the appearance of the high pressure modification $Fm\bar{3}m$, superconductivity is observed initially around 27 GPa. Upon further compression, a broad pressure region for the structural mixture exists followed by a complete $Fm\bar{3}m$ structure above about 50 GPa. Meanwhile, the critical temperature T_C first increases slightly and reaches a maximum value of about 3 K at 39.0 GPa, and then decreases gradually up to 55.0 GPa, showing a dome like $T_C - P$ superconducting phase diagram.

DISCUSSION

SnSe at ambient conditions crystallizes in an orthorhombic structure ($Pnma$) which can be described as a distortion of the simple cubic structure of NaCl. The present XRD results evidence a set of structural transitions from the low pressure $Pnma$ to $Bbmm$ (or equivalently $Cmcm$), and over a very broad pressure range further to a high pressure NaCl-type rocksalt structure ($Fm\bar{3}m$). The transition of $Pnma \rightarrow Bbmm$ mainly refers to a displacive movement of Sn/Se atoms along the $[010]$ direction (or b axis) while $Bbmm \rightarrow Fm\bar{3}m$ involves additionally Sn-Se bonding between adjacent layers, owing to anisotropic compression. Correspondingly, the nearest coordination numbers of Sn increases sequentially from three to five, and finally to six. This makes the transition of SnSe from a predominantly 2D material to a 3D network, which can also be manifested in the increasing bulk moduli under compression (Fig. 2c). Through previous structural investigations in Pb- or Sn-based IV-VI compounds[9, 20, 30], it has been a recurring theme of phase transitions: $Pnma \rightleftharpoons Bbmm$ (or $Cmcm$) $\rightleftharpoons Fm\bar{3}m$, indicating that the energy differences between these structures are fairly tiny. It thus not unexpected here that a rocksalt phase establishes for SnSe at high pressures.

The observed structural phase transitions are consistent well with the variation of resistance with pressure. In Phase I, the resistance of SnSe decreases monotonously upon compression, with the rapid closure of its band-gap (Fig. S2) followed by metallization (Fig. 3a). When SnSe entering into the $Bbmm$ phase, the magnitude of the resistance shows an abnormal upshift (Fig. 3b). Most strikingly, superconductivity is observed accompanied by the appearance of the high pressure rocksalt phase. Note that with increasing pressure, superconductivity first shows up at 27.2 GPa and zero resistance can only be observed above 34.3 GPa (see Fig. 3d). This is in agreement with the coexistence of the non-superconducting $Bbmm$ and superconducting $Fm\bar{3}m$ structures.

Recently, a large amount of efforts have been devoted to exploring the possible topological superconductors in topological materials by external pressure, such as Bi_2Se_3 [24, 44], Bi_2Te_3 [22, 45], ZrTe_5 [28], Cd_3As_2 [29], Sr doped Bi_2Se_3 [46], etc. However, one may find that the appearance of superconductivity is generally along with a structural transition, making it an open question on the topology of the pressure-induced superconducting states in these materials. In this regard, here the discovered superconductivity for SnSe rooted inherently

in the rocksalt structure at high pressures may be of particular interest. Firstly, for SnSe with a rocksalt structure, it has been theoretically predicted to be a native TCI[20]. In the epitaxial film rocksalt SnSe, Dirac surface states have been observed experimentally by ARPES[21]. Consequently, the rocksalt phase of SnSe accessed through high pressure may also possess the unique topological characteristic as it is protected only by crystal symmetry. Secondly, superconductivity is observed in the rocksalt SnSe. Several previous works in a prototypical TCI SnTe have reported that superconductivity can be achieved by substitutions[12–15]. Remarkably, surface Andreev bound states[10] were observed, which was related to odd-parity pairing and topological superconductivity[10, 11]. It is noted that the resistance in the normal state reveals temperature (below ~ 70 K) and pressure (above 39.0 GPa) independent behaviors within the experimental uncertainties. As a matter of fact, such temperature independent electronic transport behavior has also been observed in other topological materials[47, 48], which might be related to the presence of topological surface states. Considering the extreme similarities both in structural and electronic manifestations between doped SnTe and the present dense SnSe, we thus expect that the latter may also be a promising candidate to realize topological superconductivity. Obviously, more detailed understandings remain to be uncovered by further theoretical and experimental investigations.

Finally, we would like to mention that the high pressure modification of *Bbmm* SnSe resembles closely that of SnSe at elevated temperature[39], with an intersection of axes and approaching a tetragonal metric. Upon further warming, unfortunately, a sublimation happens before a possible rocksalt SnSe may generate. As a result, in addition to epitaxy-grown films[21, 49], the present study may offer an alternative strategy for synthesizing rocksalt SnSe via a combination of high pressure and high temperature techniques, and thereby test for possible topological superconductivity.

In summary, in order to search for the possible rocksalt SnSe, we performed synchrotron XRD experiments in a diamond anvil cell and indeed observed the formation of a rocksalt phase at high pressures. We found that the rocksalt phase appears at 27.3 GPa and coexists with the *Bbmm* (or equivalently *Cmcm*) phase in a broad pressure range, and eventually a pure rocksalt phase establishes above 50.1 GPa. Anisotropic compression is suggested to be responsible for the structural transitions. We further carried out electronic transport measurements to investigate the properties of the rocksalt phase. Interestingly, we observed

a pressure-driven superconductivity rooted in the rocksalt structure. It is thus proposed that the present dense SnSe may provide a model platform to investigate the topological characteristic of electronic structures and its correlation to superconductivity.

-
- [1] Fu, L. Topological crystalline insulators. *Phys. Rev. Lett.* **106**, 106802 (2011).
 - [2] Hsieh, T. H. *et al.* Topological crystalline insulators in the SnTe material class. *Nat. Commun.* **3**, 982 (2012).
 - [3] Tanaka, Y. *et al.* Experimental realization of a topological crystalline insulator in SnTe. *Nat. Phys.* **8**, 800 (2012).
 - [4] Xu, S. Y. *et al.* Observation of a topological crystalline insulator phase and topological phase transition in $\text{Pb}_{1-x}\text{Sn}_x\text{Te}$. *Nat. Commun.* **3**, 1192 (2012).
 - [5] Dziawa, P. *et al.* Topological crystalline insulator states in $\text{Pb}_{1-x}\text{Sn}_x\text{Se}$. *Nat. Mater.* **11**, 1023 (2012).
 - [6] Yan, C. H. *et al.* Experimental observation of Dirac-like surface states and topological phase transition in $\text{Pb}_{1-x}\text{Sn}_x\text{Te}$ (111) films. *Phys. Rev. Lett.* **112**, 186801 (2014).
 - [7] Ando, Y. & Fu, L. Topological Crystalline Insulators and Topological Superconductors: From Concepts to Materials. *Annu. Rev. Condens. Matter Phys.* **6**, 361-381 (2015).
 - [8] Liu, J. W. *et al.* Spin-filtered edge states with an electrically tunable gap in a two-dimensional topological crystalline insulator. *Nat. Mater.* **13**, 178 (2014).
 - [9] Zeljkovic, I. *et al.* Dirac mass generation from crystal symmetry breaking on the surfaces of topological crystalline insulators. *Nat. Mater.* **14**, 318 (2015).
 - [10] Sasaki, S. *et al.* Odd-Parity Pairing and Topological Superconductivity in a Strongly Spin-Orbit Coupled Semiconductor. *Phys. Rev. Lett.* **109**, 217004 (2012).
 - [11] Sato, T. *et al.* Fermiology of the Strongly Spin-Orbit Coupled Superconductor $\text{Sn}_{1-x}\text{In}_x\text{Te}$: Implications for Topological Superconductivity. *Phys. Rev. Lett.* **110**, 206804 (2013).
 - [12] Balakrishnan, G. *et al.* Superconducting properties of the In-substituted topological crystalline insulator SnTe. *Phys. Rev. B* **87**, 140507(R) (2013).
 - [13] Maurya, V. K. *et al.* Electromagnetic Properties of Topological Crystalline Superconductor $\text{Sn}_{0.5}\text{In}_{0.5}\text{Te}$. preprint at *arXiv:1406.2155*.
 - [14] Mizuguchi, Y. *et al.* Specific Heat and Electrical Transport Properties of $\text{Sn}_{0.8}\text{Ag}_{0.2}\text{Te}$ Super-

- conductor. preprint at *arXiv:1607.05474*.
- [15] Zhong, R. D *et al.* Superconductivity induced by In substitution into the topological crystalline insulator $\text{Pb}_{0.5}\text{Sn}_{0.5}\text{Te}$. *Phys. Rev. B* **90**, 020505(R) (2014).
 - [16] Das, S. *et al.* Unexpected superconductivity at nanoscale junctions made on the topological crystalline insulator $\text{Pb}_{0.6}\text{Sn}_{0.4}\text{Te}$. preprint at *arXiv:1607.01609v1*.
 - [17] Zhao, L. D. *et al.* Ultralow thermal conductivity and high thermoelectric figure of merit in SnSe crystals. *Nature* **508**, 373-377 (2014).
 - [18] Zhao, L. D. *et al.* Ultrahigh power factor and thermoelectric performance in hole-doped single-crystal SnSe. *Science* **351**, 141-144 (2016).
 - [19] Neupane, M. *et al.* Topological phase diagram and saddle point singularity in a tunable topological crystalline insulator. *Phys. Rev. B* **92**, 075131 (2015).
 - [20] Sun, Y. *et al.* Rocksalt SnS and SnSe: Native topological crystalline insulators. *Phys. Rev. B* **88**, 235122 (2013).
 - [21] Wang, Z. Y. *et al.* Molecular Beam Epitaxy-Grown SnSe in the Rock-Salt Structure: An Artificial Topological Crystalline Insulator Material. *Adv. Mater.* **27**, 4150-4154 (2015).
 - [22] Zhang, J. L. *et al.* Pressure-induced superconductivity in topological parent compound Bi_2Te_3 . *Proc. Natl. Acad. Sci. U.S.A.* **108**, 24 (2011).
 - [23] Zhang, C. *et al.* Phase diagram of a pressure-induced superconducting state and its relation to the Hall coefficient of Bi_2Te_3 single crystals. *Phys. Rev. B* **83**, 140504(R) (2011).
 - [24] Kirshenbaum, K. *et al.* Pressure-induced unconventional superconducting phase in the topological insulator Bi_2Se_3 . *Phys. Rev. Lett.* **111**, 087001 (2013).
 - [25] Kang, D. F. *et al.* Superconductivity emerging from a suppressed large magnetoresistant state in tungsten ditelluride. *Nat. Commun.* **6**, 7804 (2015).
 - [26] Pan, X. C. *et al.* Pressure-driven dome-shaped superconductivity and electronic structural evolution in tungsten ditelluride. *Nat. Commun.* **6**, 7805 (2015).
 - [27] Qi, Y. P. *et al.* Superconductivity in Weyl semimetal candidate MoTe_2 . *Nat. Commun.* **7**, 11038 (2016).
 - [28] Zhou, Y. H. *et al.* Pressure-induced superconductivity in a three-dimensional topological material ZrTe_5 . *Proc. Natl. Acad. Sci. USA* **113**, 2904-2909 (2016).
 - [29] He, L. P. *et al.* Pressure-induced superconductivity in the three-dimensional topological Dirac semimetal Cd_3As_2 . preprint at *arXiv:1502.02059*.

- [30] Chattopadhyay, T., Werner, A. & von Schnering, H. G. Temperature and pressure induced phase transition in IV-VI compounds. *Revue Phys. Appl.* **19**, 807-813 (1984).
- [31] Loa, I. *et al.* Structural changes in thermoelectric SnSe at high pressures. *J. Phys.: Condens. Matter* **27**, 072202 (2015).
- [32] Zhang, J. *et al.* Plasma-assisted synthesis and pressure-induced structural transition of single-crystalline SnSe nanosheets. *Nanoscale* **7**, 10807-10816 (2015).
- [33] de Souza, S. M. *et al.* Pressure-induced polymorphism in nanostructured SnSe. *J. Appl. Cryst.* **49**, 213-221 (2016).
- [34] Alptekin, S. Structural phase transition of SnSe under uniaxial stress and hydrostatic pressure: an *ab initio* study. *J. Mol. Model* **17**, 2989-2994 (2011).
- [35] Makinistian, L. & Albanesi, E. A. Study of the hydrostatic pressure on orthorhombic IV-VI compounds including many-body effects. *Computational Materials Science* **50**, 2872-2879 (2011).
- [36] Yan, J. J. *et al.* Pressure-driven semiconducting-semimetallic transition in SnSe. *Phys. Chem. Chem. Phys.* **18**, 5012-5018 (2016).
- [37] Von Dreele, R. B. & Larson, A. C. General structure analysis system. *Regents of the University of California* (2001); Toby, B. H. EXPGUI, a graphical user interface for GSAS. *J. Appl. Cryst.* **34**, 210-213 (2001).
- [38] Chattopadhyay, T. *et al.* Neutron diffraction study of the structural phase transition in SnS and SnSe. *J. Phys. Chem. Solids* **47**, 879-885 (1986).
- [39] Wiedemeier, H. & Csillag, F. J. The thermal expansion and high temperature transformation of SnS and SnSe. *Zeitschrift für Kristallographie* **149**, 17-29 (1979).
- [40] Birch, F. Finite Elastic Strain of Cubic Crystals. *Phys. Rev.* **71**, 809-824 (1947).
- [41] Smith, P. L. & Martin, J. E. The high-pressure structures of zinc sulphide and zinc selenide. *Phys. Lett.* **39**, 541-543 (1965).
- [42] Zhou, Y. H. *et al.* Pressure-induced Td to $1T'$ structural phase transition in WTe_2 . *AIP Adv.* **6**, 075008 (2016).
- [43] Nassary, M. M. The electrical conduction mechanisms and thermoelectric power of SnSe single crystals. *Turk. J. Phys.* **33**, 201-208 (2009).
- [44] Yu, Z. H. *et al.* Structural phase transitions in Bi_2Se_3 under high pressure. *Sci. Rep.* **5**, 15939 (2015).

- [45] Matsubayashi, K. *et al.* Superconductivity in the topological insulator Bi_2Te_3 under hydrostatic pressure. *Phys. Rev. B* **90**, 125126 (2014).
- [46] Zhou, Y. H. *et al.* Pressure-induced reemergence of superconductivity in topological insulator $\text{Sr}_{0.065}\text{Bi}_2\text{Se}_3$. *Phys. Rev. B* **93**, 144514 (2016).
- [47] Gabáni, S. *et al.* Pressure-induced Fermi-liquid behavior in the Kondo insulator SmB_6 : Possible transition through a quantum critical point. *Phys. Rev. B* **67**, 172406 (2013).
- [48] Tafti, F. F. *et al.* Resistivity plateau and extreme magnetoresistance in LaSb . *Nat. Phys.* **12**, 272-277 (2015).
- [49] Mariano, A. N. & Chopra, K. L. Polymorphism in some IV-VI compounds induced by high pressure and thin-film epitaxial growth. *Appl. Phys. Lett.* **10**, 282-284 (1967).
- [50] Park, C. Y. *et al.* New developments in micro-X-ray diffraction and X-ray absorption spectroscopy for high-pressure research at 16-BM-D at the Advanced Photon Source. *Rev. Sci. Instrum.* **86**, 072205 (2015).
- [51] Prescher, C. & Prakapenka, V. B. DIOPTAS: a program for reduction of two-dimensional X-ray diffraction data and data exploration. *High Pressure Research* **35**, 223-230 (2015).
- [52] Mao, H. K., Xu, J. & Bell, P. M. Calibration of the ruby pressure gauge to 800 kbar under quasi-hydrostatic conditions. *J. Geophys. Res.* **91**, 4673-4676 (1986).

METHODS

Sample growth: High-quality single crystals of SnSe were grown by a chemical vapor transport method. Firstly, the polycrystalline powders were synthesized by a solid-state reaction using elemental Sn (Alfa Aesar 99.8%) and Se (Alfa Aesar 99.5%) in sealed and evacuated quartz ampoules. The stoichiometric amounts of mixture were heated to 700°C in rate of 3 K/min and maintained at this temperature for 3 days. Then the SnSe powder was sealed in a quartz tube under vacuum and kept in a temperature gradient 700°C to 800°C for 7 days. SnSe single crystals were obtained at the hot end. The laboratory X-ray diffraction measurements, which were done at room temperature using $\text{Cu } K_\alpha$ radiation on Rigaku TTR3 diffractometer, have proven that the obtained crystals are single phase with the orthorhombic structure of space group $Pnma$.

High Pressure experiments: High-pressure resistance experiments were conducted

in a diamond anvil cell made of Pe-Cu alloy[26] using sodium chloride (NaCl) powder as the pressure-transmitting medium. SnSe single crystal was cleaved along the [100] direction then a tiny sheet of $100\mu m \times 50\mu m \times 10\mu m$ was loaded together with a ruby ball. The standard four-probe method was employed to measure the resistance. High-pressure synchrotron X-ray diffraction (XRD) measurements were performed in a Mao-Bell cell at 16-BM-D, HPCAT[50] at Advanced Photon Source of Argonne National Laboratory. The X-ray wavelength is 0.4246 Å and Daphne 7373 was used as the pressure medium. A two dimensional area detector Mar345 was used to collect the powder diffraction patterns. The Dioptas[51] and GSAS+EXPGUI programs[37] were employed for image integrations and XRD profile Rietveld refinements, respectively. Pressure was calibrated by using the ruby fluorescence shift at room temperature[52].

ACKNOWLEDGEMENTS

The authors would like to thank Prof. Xianhui Chen for stimulating discussions. This work is supported by the Ministry of Science and Technology of China (National Basic Research Program Nos. 2016YFA0300404 and 2016YFA0401804), and the National Natural Science Foundation of China (Grant Nos. 11572343, 11474288, 51472036, U1332143). Y.X. thanks the support of the Hundred Talents Program of the Chinese Academy of Science. The X-ray work was performed at HPCAT (Sector 16), Advanced Photon Source (APS), Argonne National Laboratory. HPCAT operations are supported by DOE-NNSA under Award No. de-na0001974 and DOE-BES under Award No. DE-FG02-99ER45775, with partial instrumentation funding by NSF. The Advanced Photon Source is a U.S. Department of Energy (DOE) Office of Science User Facility operated for the DOE Office of Science by Argonne National Laboratory under Contract No. DE-AC02-06CH11357.

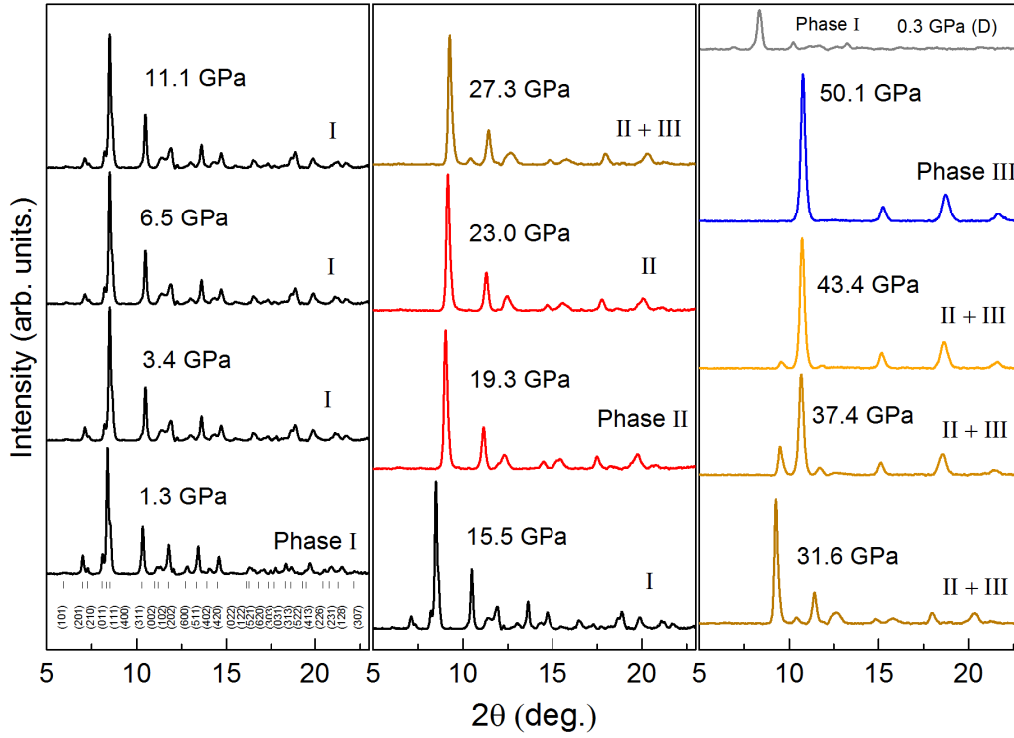


FIG. 1: *In situ* high pressure synchrotron X-ray diffraction patterns of SnSe. The patterns were recorded at room temperature with a wavelength of $\lambda = 0.4246 \text{ \AA}$. Upon compression, the patterns can be well indexed by space groups $Pnma$ (No. 62, below 15.5 GPa, Phase I), $Bbmm$ (No. 63, between 19.3 and 23.0 GPa, Phase II) and $Fm\bar{3}m$ (No. 225, above 50.1 GPa, Phase III). In the pressure range of 27.3-43.4 GPa, the XRD patterns contains a mixture of Phase II and III. When decompressing back to 0.3 GPa (denoted by D), the XRD pattern came back to the starting structure, manifesting that the pressure-driven structural transition is reversible.

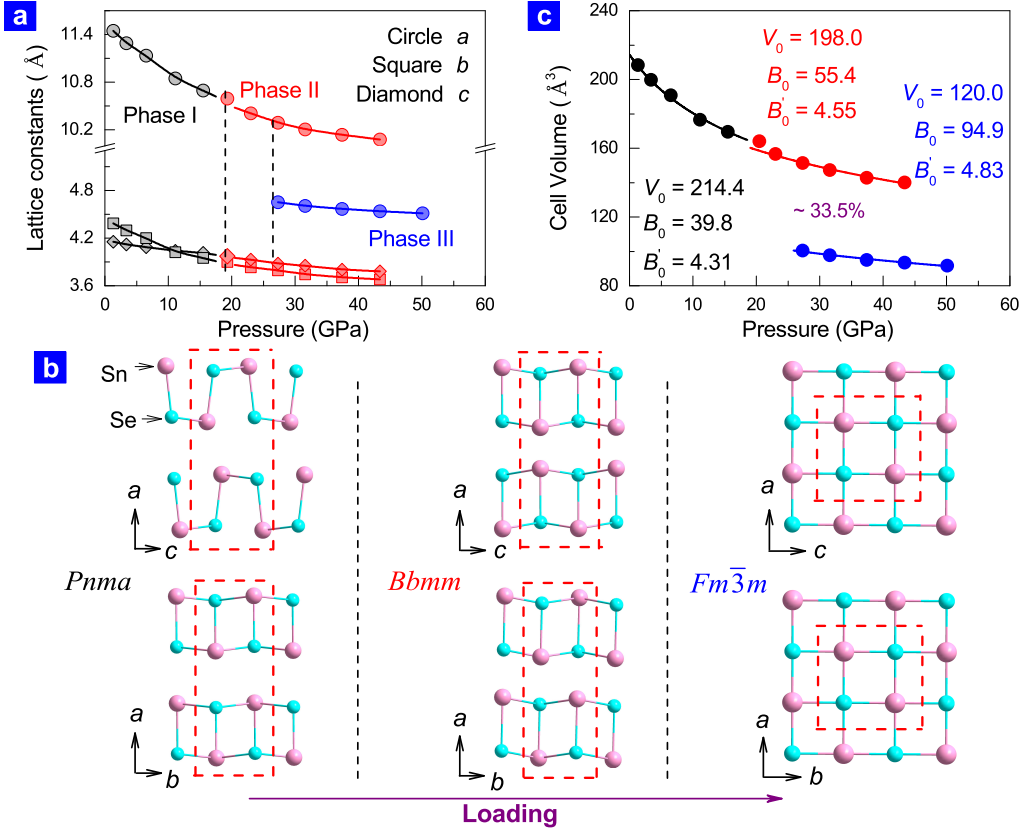


FIG. 2: **Structural parameters of SnSe under pressure.** **a** Lattice parameters as a function of pressure. The continuous and dis-continuous changes at the low and high critical pressures (vertical dashed lines) indicate that the transitions are of second and first orders in nature, respectively. **b** Crystal structures of SnSe at 1.3 GPa ($Pnma$, left), 19.3 GPa ($Bbmm$, middle) and 50.1 GPa ($Fm\bar{3}m$, right) during loading. The dashed rectangles indicate the unit cell edges. **c** The compression data was fitted by the third order Birch-Murnaghan equation of state (solid lines), which yields the bulk modulus B_0 and its first order derivative B'_0 : 39.8, 4.31; 55.4, 4.55; 94.9, 4.83 for the $Pnma$, $Bbmm$ and $Fm\bar{3}m$ phases. Over the transitions, the unit cells collapse about 2% (low critical pressure) and 33.5% (high critical pressure).

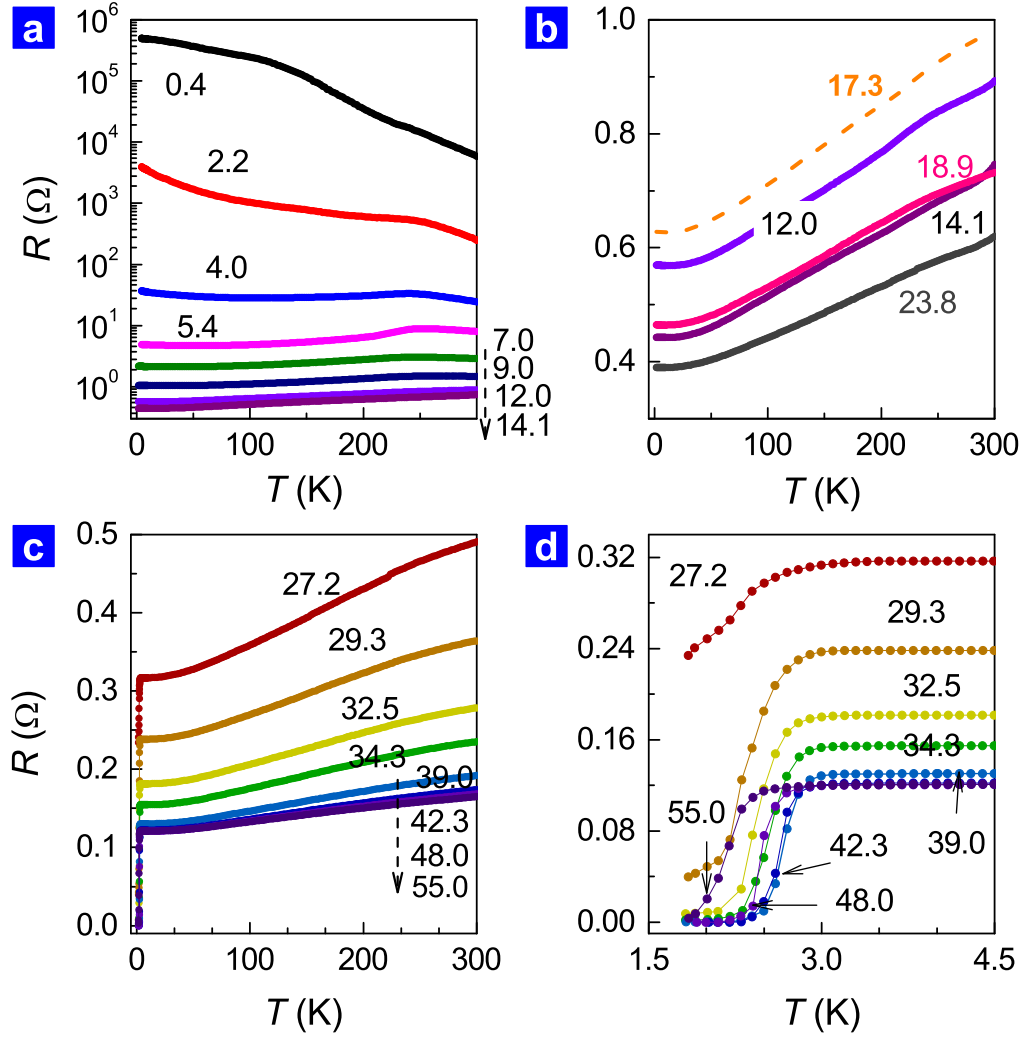


FIG. 3: **Experimental evidence for pressure induced superconductivity.** **a-c** Temperature dependent resistance for SnSe single crystal. **d** An enlarged view of the low temperature resistance above 27.2 GPa showing the superconducting transition. Note that the magnitude of the resistance at 17.3 GPa enhances abruptly in the whole temperature region as indicated by the dashed line in **b**, and then decreases gradually followed by an almost unchangeable behavior above 39.0 GPa.

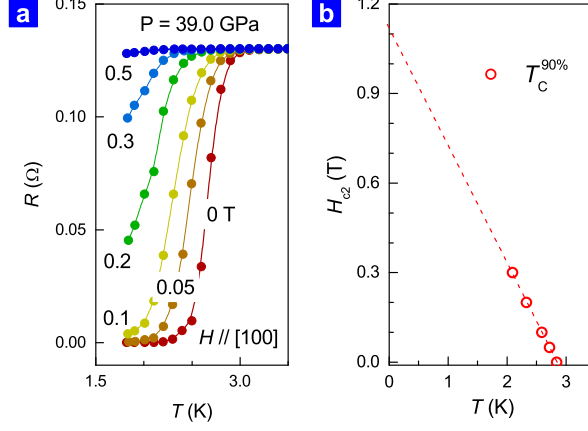


FIG. 4: **The upper critical field H_{C2} of SnSe under 39.0 GPa.** **a** The superconducting transition of the SnSe single crystal in magnetic fields up to 0.5 T. The applied magnetic field is parallel to the $[100]$ direction of SnSe single crystal. **b** Temperature dependence of the upper critical field H_{C2} . T_C is determined as the 90% drop of the normal state resistance. The dashed line is a linear fit to the data and $H_{C2}(0)$ is estimated to be 1.12 T.

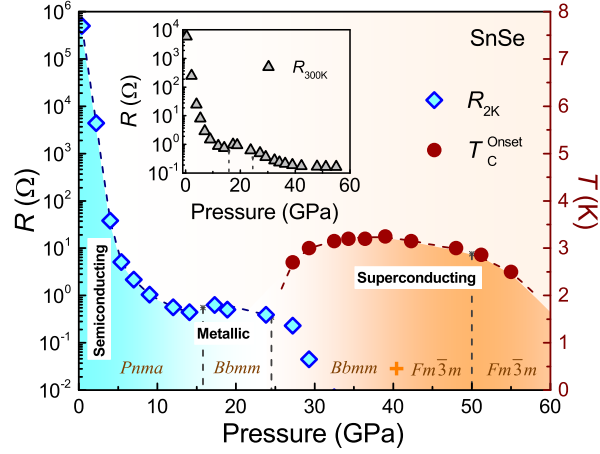


FIG. 5: **Phase diagram of SnSe.** Temperature versus pressure phase diagram. The left axis stands for the resistance R at 2 K and the right axis corresponds to temperature T . The high pressure phase of SnSe is found to be $Fm\bar{3}m$ structure, a so-called rocksalt NaCl-type, which may be a possible topological crystalline insulator. Upon compression, superconductivity is initially observed accompanied by the occurrence of the rock-salt structure embedded in the $Bbmm$ phase. The critical temperature T_C , defined as the onset of the superconducting transition, first increases slightly, then maximizes at about 39 GPa and finally decreases gradually up to the highest pressure of 50.1 GPa achieved in the present experiments, revealing a dome-like $T_C - P$ phase diagram.

Supplementary Information

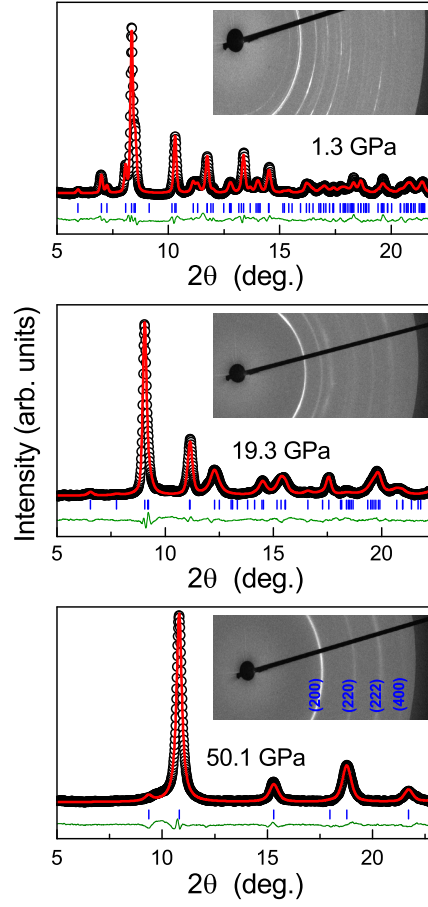


FIG. S1: **Fits of X-ray diffraction profiles.** Standard Rietveld method was used to fit the data and the refinements were performed using the GSAS program[37]. Representative experimental raw images (partial) for each phase are also displayed.

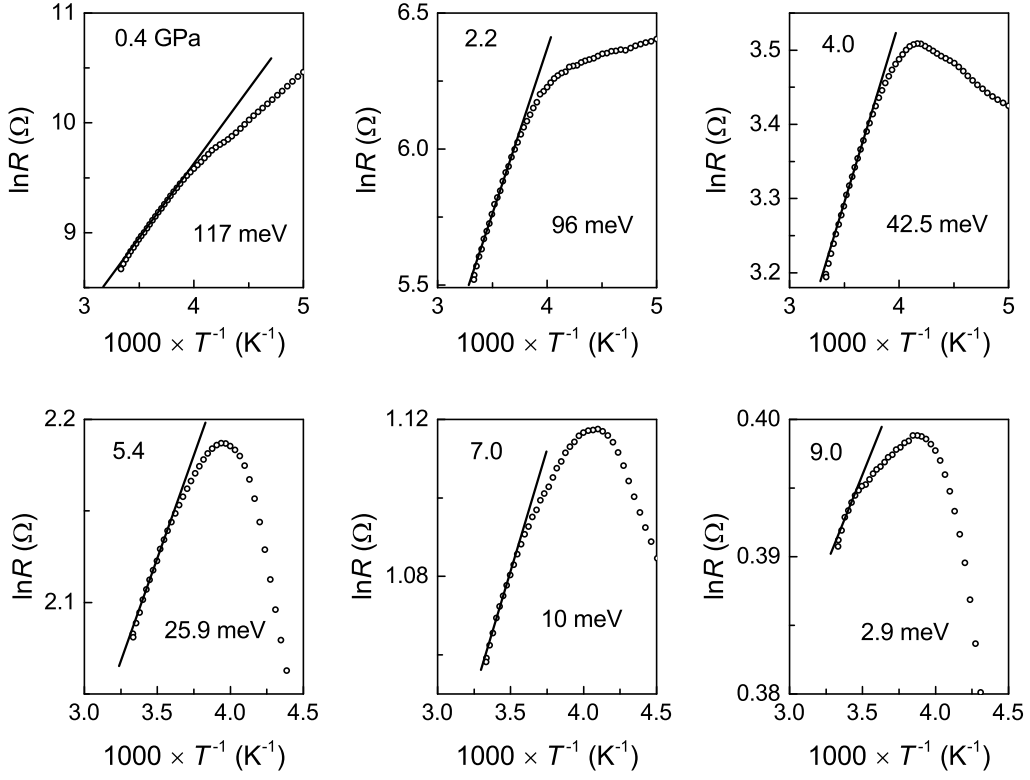


FIG. S2: **Fitting of energy gap under pressure.** The data is displayed in the representative of $\ln R$ versus $1000/T$. The measured DC resistance R is fitted by the well-known Arrhenius relationship of $R = R_0 \times \exp(\frac{\Delta E}{k_B T})$, where R_0 is a pre-exponential factor and ΔE represents the activation energy, k_B is the Boltzmann constant and T is the absolute temperature.

TABLE S1: Results of the Rietveld refinements of SnSe at 1.3, 19.3, and 50.1 GPa: lattice parameters a - c ; the number of chemical formulas contained in the unit cell Z ; fractional coordinates x , y and z of the Sn and Se positions; isotropic atomic displacement parameters U_{iso} ; refined values R_{WP} , R_P , χ^2 .

	Phase I: $Pnma$	Phase II: $Bbmm$	Phase III: $Fm\bar{3}m$
Parameters	1.3 GPa	19.3GPa	50.1GPa
$a(\text{\AA})$	11.4473(9)	10.5928(2)	4.5095(3)
$b(\text{\AA})$	4.1517(1)	3.9003(3)	4.5095(3)
$c(\text{\AA})$	4.3865(2)	3.9716(6)	4.5095(3)
Z	4	4	4
$x(\text{Sn/Se})$ (f.c.)	0.1214(3)/0.8575(5)	0.8983(12)/0.1331(5)	0/0.5
$y(\text{Sn/Se})$ (f.c.)	0.25/0.25	0.25/0.25	0/0.5
$z(\text{Sn/Se})$ (f.c.)	0.9095(7)/0.5176(8)	0.5/0	0/0.5
$U_{iso}(\text{\AA}^2)$	0.032(0)/0.01	0.036(0)/0.01	0.048(1)/0.01
R_{WP} , R_P , χ^2	0.77%, 0.6%, 0.044	0.66%, 0.49%, 0.031	0.75%, 0.51%, 0.037

Note: The atomic displacement parameter $U_{iso}(\text{Se})$ was fixed at 0.01 \AA^2 since it would otherwise refine to negative values.